Novel Algorithms for High-Accuracy Joint Position and Orientation Estimation in 5G mmWave Systems"

Novel Algorithms for High-Accuracy Joint Position and Orientation Estimation in 5G mmWave Systems

Jukka Talvitie*, Mikko Valkama*, Giuseppe Destino†, Henk Wymeersch‡
*Laboratory of Electronics and Communications Engineering, Tampere University of Technology, Finland
†Centre for Wireless Communications, University of Oulu, Finland
‡ Department of Electrical Engineering, Chalmers University of Technology, Sweden
Email: jukka.talvitie@tut.fi

***Abstract*—We propose a method for accurate estimation of the User Equipment (UE) position and antenna orientation. For this, we exploit the sparsity of the mm-wave channel, and employ a compressive sensing approach with iterative refinement steps for accurate estimation of the channel parameters, including the departure and arrival angles as well as the time-of-arrival for each observed propagation path. Based on the estimated channel parameters, we formulate an iterative Gibbs sampler to obtain statistical descriptions for the unknown UE position and orientation along with the unknown scatterer positions, even in the absence of a Line-Of-Sight path.**

***Keywords*—Positioning, 5G mobile networks, Mm-wave, MIMO, Compressed sensing, Gibbs sampler, Joint estimation**

I. Introduction

Millimeter-wave (mm-wave) communications operate in the spectrum above 28 GHz and are expected to provide fiber-like data rates for future 5G systems [1], [2]. By utilizing large antenna arrays and beamforming at both transmitter and receiver side, high-SNR links with large bandwidths are created. An important property of mm-wave communication is channel sparsity: due to the high path loss, limited shadowing and diffraction, only a limited number of propagation paths reach from the transmitter to the receiver. This sparsity can be harnessed for channel estimation [3]–[7] as well as precoding and combining [8]–[10].

The specific properties of mm-wave communications (large bandwidth, sparse channel, and large antenna arrays) are of great interest to the area of radio-based localization. In [11], the potential of mm-wave 5G positioning system was studied by exploiting the information on the Non-Line-Of-Sight (NLOS) paths and channel geometry. Furthermore, the assumption of channel sparsity has been used for positioning purposes in [7], [12], [13], where in the latter also the User Equipment (UE) orientation estimation has been considered. In addition to these, analytical bounds for the position and orientation estimation error has been studied in [14].

In this paper, we provide a novel method for joint position and orientation estimation from a single reference device. Our approach includes sparsity-based channel estimation method with an adaptive dictionary [12], followed by a recursive Gibbs sampler, operating in the joint position and orientation space. The proposed method has a number of attractive properties: it does not require prior knowledge on the number of paths, it does not require a Line-Of-Sight (LOS) path or even knowledge of the existence of a LOS path, it provides a statistical description of the user's location and orientation, as well as of scatterers. As such, the proposed method can be extended to a Simultaneous Localization and Mapping (SLAM) setting, or a tracking scenario, including use cases from pedestrian and vehicular transport to navigation of Unmanned Autonomous Vehicles (UAV). Also, the proposed algorithm requires only the connection to one Base Station (BS). From a system level viewpoint, this feature is the key to overcome limiting factors of the previous generation of mobile network positioning, such as synchronization, scheduling and interference management. In addition, the proposed approach can be straightforwardly extended to an uplink scenario.

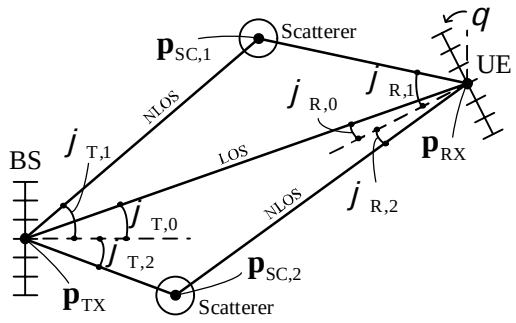

Fig. 1. An example scenario of a LOS path and 2 NLOS paths including the AOD and AOA for each path. The AOAs are affected by the unknown orientation of the UE.

II. System model

We study a Multiple-Input Multiple-Output (MIMO) system including a BS at a known position $\mathbf{p}_{\text{TX}} \in \mathbb{R}^2$ with a known antenna orientation, and a UE at an unknown position $\mathbf{p}_{\text{RX}} \in \mathbb{R}^2$ with an unknown antenna orientation θ. The BS transmits a sequence of M Orthogonal Frequency-Division Multiplexing (OFDM) symbols on N active subcarriers, where $\mathbf{x}[m,n] = [x_0[m,n], ..., x_{N_\text{b}-1}[m,n]]^T$ denotes simultaneously transmitted subcarrier-wise symbols at n^{th} subcarrier and m^{th} OFDM symbol with N_b digital paths. To model a wideband OFDM transmission, we apply a MIMO channel model described in [15]. Moreover, we assume that the channel remains constant during the sequence of M transmitted OFDM symbols. Now, for each subcarrier n the MIMO channel matrix $\mathbf{H}[n] \in \mathbb{C}^{N_\text{R} \times N_\text{T}}$, in which N_T and N_R are the number of transmit and receive antennas, is given as

$$\mathbf{H}[n] = \mathbf{A}_\text{R}[n]\mathbf{\Gamma}[n]\mathbf{A}_\text{T}^H[n], \text{ where} \quad (1)$$

$$\begin{aligned}\mathbf{A}_{\mathrm{T}}[n] &= [\mathbf{a}_{\mathrm{T},n}(\varphi_{\mathrm{T},0}), ..., \mathbf{a}_{\mathrm{T},n}(\varphi_{\mathrm{R},K-1})] \text{ and} \\ \mathbf{A}_{\mathrm{R}}[n] &= [\mathbf{a}_{\mathrm{R},n}(\varphi_{\mathrm{R},0}), ..., \mathbf{a}_{\mathrm{R},n}(\varphi_{\mathrm{R},K-1})]\end{aligned} \tag{2}$$

are steering vector matrices which introduce the Angle-Of-Departure (AOD) $\varphi_{\mathrm{R},k}$, Angle-Of-Arrival (AOA) $\varphi_{\mathrm{T},k}$, and Time-Of-Arrival (TOA) τ_k for each path $k = 0, ..., K-1$, and K is the number of observable paths. In case that the LOS path exists, it is always defined as the first path with $k = 0$, as illustrated in the example scenario in Fig. 1. In addition, $\mathbf{\Gamma}[n] = [\gamma_0, ..., \gamma_{K-1}]$ is a diagonal channel coefficient matrix whose k^{th} diagonal element is defined as

$$\gamma_k = \sqrt{N_{\mathrm{T}} N_{\mathrm{R}}} \frac{h_k}{\sqrt{\eta_k}} e^{-j2\pi\tau_k/(NT_s)}. \tag{3}$$

Here h_k, η_k and τ_k are the complex channel coefficient, the path loss coefficient and the TOA of the k^{th} path, respectively. Moreover, $T_s = 1/B$ is the sample duration, where B is the bandwidth of the OFDM signal passband. In addition, throughout the paper we consider a uniform linear array antenna structure with antenna separation of d_{ant}. Consequently, the steering vector $\mathbf{a}_{\mathrm{T},n}(\varphi_{\mathrm{T},0})$ (and similarly for $\mathbf{a}_{\mathrm{R},n}(\varphi_{\mathrm{R},0})$) is given as

$$\mathbf{a}_{\mathrm{T},n}(\varphi_{\mathrm{T},k}) = \frac{1}{\sqrt{N_{\mathrm{T}}}} \left[e^{-j\frac{N_{\mathrm{T}}-1}{2}\Phi(\varphi_{\mathrm{T},k})}, ..., e^{j\frac{N_{\mathrm{T}}-1}{2}\Phi(\varphi_{\mathrm{T},k})} \right] \tag{4}$$

where $\Phi(\varphi_{\mathrm{T},k}) = 2\pi d_{\text{ant}}/\lambda_n \sin(\varphi_{\mathrm{T},k})$ describes the electrical angle corresponding to the physical angle $\varphi_{\mathrm{T},k}$, and λ_n is the wavelength of the n^{th} subcarrier.

By assuming ideal sampling and cyclic prefix (CP) removal, and after taking the Fast Fourier Transform (FFT), the received sample of the m^{th} OFDM symbol and n^{th} subcarrier can be written as

$$\mathbf{y}[m, n] = \mathbf{H}[n]\mathbf{F}[m, n]\mathbf{x}[m, n] + \mathbf{n}[m, n], \tag{5}$$

where $\mathbf{n}[m, n]$ is zero mean complex Gaussian noise and $\mathbf{F}[m, n] \in \mathbb{C}^{N_{\mathrm{T}} \times N_{\mathrm{b}}}$ is a beamforming matrix, known by the UE.

III. Channel parameter estimation

To estimate the channel parameters AOD, AOA and TOA, we exploit the above discussed sparsity of the mm-wave channel. For this, we utilize the Distributed Compressed Sensing - Simultaneous Orthogonal Matching Pursuit (DCS-SOMP) method presented in [16]. Then, based on the DCS-SOMP output, we use a novel iterative refinement method to increase the estimation accuracy up to a desired level with feasible computational complexity.

A. Sparse beamspace channel representation

The transformation from the conventional MIMO channel matrix to an angular domain beamspace matrix $\mathbf{H}_{\varphi}[n] \in \mathbb{C}^{N_{\mathrm{R}} \times N_{\mathrm{T}}}$ can be achieved by

$$\mathbf{H}_{\varphi}[n] = \mathbf{U}_{\mathrm{R}}^{H} \mathbf{H}[n] \mathbf{U}_{\mathrm{T}}, \tag{6}$$

where $\mathbf{U}_{\mathrm{T}}$ and $\mathbf{U}_{\mathrm{R}}$ are transformation matrices, which are chosen based on the desired angular space representation. For example, by considering an Uniform Linear Array (ULA) antenna model, to span the beamspace with uniformly sampled angles, $\mathbf{U}_{\mathrm{T}}$ (and similarly $\mathbf{U}_{\mathrm{R}}$) is defined as

$$\begin{aligned}\mathbf{U}_{\mathrm{T}} &= [\mathbf{u}_{\mathrm{T}}(\nu_0), ..., \mathbf{u}_{\mathrm{T}}(\nu_{N_{\mathrm{T}}-1})], \text{ where} \\ \mathbf{u}_{\mathrm{T}}(\nu_l) &= \left[e^{-j2\pi\frac{N_{\mathrm{T}}-1}{2}\nu_l}, ..., e^{j2\pi\frac{N_{\mathrm{T}}-1}{2}\nu_l} \right]^T, \text{ and} \\ \nu_l &= -\frac{N_{\mathrm{T}}-1}{2N_{\mathrm{T}}} + \frac{l}{N_{\mathrm{T}}},\end{aligned} \tag{7}$$

where the beamspace angles are defined by the beamspace grid vector $\boldsymbol{\nu} = [\nu_0, ...\nu_{N_{\mathrm{T}}-1}]$. Based on this, the beamspace angle resolution for the AOD and AOA are defined as $\kappa_{\mathrm{T}} = 1/N_{\mathrm{T}}$ and $\kappa_{\mathrm{R}} = 1/N_{\mathrm{R}}$. Now, as indicated in [17], this beamspace is nearly sparse and it introduces significant energy only in the neighborhood of the AOD and AOA.

By employing the beamspace representation in (6) the vectorization of the received samples defined in (5) results in

$$\begin{aligned}\mathbf{y}_{\varphi}[n] &= \mathbf{\Omega}[n]\mathbf{h}_{\varphi}[n] + \mathbf{n}_{\varphi}[n], \text{ where} \\ \mathbf{\Omega}[n] &= [\mathbf{\Omega}_{0,n}, ..., \mathbf{\Omega}_{M-1,n}]^T \text{ with} \\ \mathbf{\Omega}_{m,n} &= \left(\mathbf{U}_{\mathrm{T}}^{H}\mathbf{F}[m, n]\mathbf{x}[m, n]\right)^T \otimes \mathbf{U}_{\mathrm{R}}, \text{ and} \\ \mathbf{h}_{\varphi}[n] &= \text{vec}(\mathbf{H}_{\varphi}[n]),\end{aligned} \tag{8}$$

where $\mathbf{h}_{\varphi}[n]$ is the nearly sparse channel vector, and $\mathbf{\Omega}[n]$ is a dictionary (or sensing) matrix whose columns depend on different combinations of channel AOD and AOA values. Furthermore, as $\mathbf{\Omega}[n]$ and $\mathbf{h}_{\varphi}[n]$ have a common support over all subcarriers, the channel parameter estimation can be carried out efficiently via the distributed compressed sensing approach.

B. Estimation of AOA and AOD

In order to estimate the channel parameters $\varphi_{\mathrm{T},k}$, $\varphi_{\mathrm{R},k}$ (and later τ_k) for $k = 0, ..., K-1$, we use the DCS-SOMP method given in [16]. The steps of the DCS-SOMP algorithm are described as follows:

1) Initialize by setting the residual vector $\mathbf{r}_{-1}[n] = \mathbf{y}_{\varphi}[n]$ and the iteration index $s = 0$.
2) Search for the coarse estimates of AOD $\tilde{\varphi}_{\mathrm{T},s}$ and AOA $\tilde{\varphi}_{\mathrm{R},s}$:

$$\tilde{q}_s = \underset{i=0,...,N_{\mathbf{\Omega}}-1}{\arg\max} \sum_{n=0}^{N-1} \frac{|\boldsymbol{\omega}_i^H[n]\mathbf{r}_{s-1}[n]|}{\|\boldsymbol{\omega}_i[n]\|}, \text{ where} \tag{9}$$

$$q_{\mathrm{T},s} = \left\lceil \frac{\tilde{q}_s}{N_{\mathrm{R}}} \right\rceil - 1 \text{ and } q_{\mathrm{R},s} = \text{mod}(\tilde{q}_s - 1, N_{\mathrm{R}}) \tag{10}$$

and

$$\begin{aligned}\tilde{\varphi}_{\mathrm{T},s} &= \arcsin\left(\frac{\lambda_c}{d_{\text{ant}} N_{\mathrm{T}}} \left(q_{\mathrm{T},s} - \frac{N_{\mathrm{T}}-1}{2} \right) \right), \\ \tilde{\varphi}_{\mathrm{R},s} &= \arcsin\left(\frac{\lambda_c}{d_{\text{ant}} N_{\mathrm{R}}} \left(q_{\mathrm{R},s} - \frac{N_{\mathrm{R}}-1}{2} \right) \right),\end{aligned} \tag{11}$$

where $\boldsymbol{\omega}_i[n]$ is the i^{th} column of $\mathbf{\Omega}[n]$ with $i = 0, ..., N_{\mathbf{\Omega}} - 1$, $\tilde{q}_s$ denotes the column index of the found path, and $q_{\mathrm{T},s}$ along with $q_{\mathrm{R},s}$ refer to the corresponding AOD and AOD angle indices in the used beamspace, respectively.
3) Determine a new basis vector $\boldsymbol{\psi}_s[n]$ (with assumption of $\boldsymbol{\psi}_{-1}[n] = 0$) for the desired sparse representation

by orthogonalizing the found column vector $\boldsymbol{\omega}_{\tilde{q}_s}[n]$ with respect to the earlier found basis vectors :

$$\boldsymbol{\psi}_s[n] = \boldsymbol{\omega}_{\tilde{q}_s}[n] - \sum_{\tilde{s}=-1}^{s-1} \frac{\boldsymbol{\omega}_{\tilde{q}_s}^H[n]\boldsymbol{\psi}_{\tilde{s}}[n]}{\|\boldsymbol{\psi}_{\tilde{s}}[n]\|}\boldsymbol{\psi}_{\tilde{s}}[n]. \quad (12)$$

4) Update the residual vector by removing the projection of $\boldsymbol{\psi}_s[n]$ from the space spanned by $\mathbf{r}_{s-1}[n]$:

$$\mathbf{r}_s[n] = \mathbf{r}_{s-1}[n] - \beta_s[n]\boldsymbol{\psi}_s[n], \text{ where} \quad (13)$$

$$\beta_s[n] = \frac{\boldsymbol{\psi}_s^H[n]\mathbf{r}_{s-1}[n]}{\|\boldsymbol{\psi}_s\|^2}. \quad (14)$$

5) Check the validity of the convergence criterion, that is, $\sum_{n=0}^{N-1} \|\mathbf{r}_s[n] - \mathbf{r}_{s-1}[n]\|^2 \leq \varepsilon$, where ε is a predetermined threshold value determined based on the estimated SNR. If not converged, set $s = s + 1$ and continue from the step 2. Otherwise, stop the iterations with the $\hat{K} = s + 1$ found paths.

By fixing the number of paths based on the output of the DCS-SOMP algorithm, we attempt to improve the estimation accuracy by re-defining the beamspace transformation matrices $\mathbf{U}_{\mathrm{T}}$ and $\mathbf{U}_{\mathrm{R}}$ in (8) with increased angle resolution. Now, for each found path $k = 0, ..., \hat{K}-1$, we improve the coarse angle estimates $\tilde{\varphi}_{\mathrm{T},k}$ and $\tilde{\varphi}_{\mathrm{R},k}$ by conducting an iterative refinement algorithm as follows:

1) Initialize by setting the iteration index $s = 1$, and define the beamspace AOD and AOA estimates as $\breve{\varphi}_{\mathrm{T},k}^{(0)} = \nu_{q_{\mathrm{T},k}}$ and $\breve{\varphi}_{\mathrm{R},k}^{(0)} = \nu_{q_{\mathrm{R},k}}$ based on (7) and (10). In addition, define the initial beamspace resolution for AOD and AOA as $\tilde{\kappa}_{\mathrm{T}}^{(0)} = \kappa_{\mathrm{T}}$ and $\tilde{\kappa}_{\mathrm{R}}^{(0)} = \kappa_{\mathrm{R}}$.
2) Re-define the beamspace transformation matrices by quadrupling the angle resolution by setting $\tilde{\kappa}_{\mathrm{T},s} = \tilde{\kappa}_{\mathrm{T},s-1}/4$, and create a new beamspace grid around the estimated AOD and AOA values as

$$\begin{aligned} \tilde{\mathbf{U}}_{\mathrm{T},k}^{(s)} &= \left[\mathbf{u}_{\mathrm{T}}(\tilde{\nu}_{0,k}^{(s)}), ..., \mathbf{u}_{\mathrm{T}}(\tilde{\nu}_{4,k}^{(s)})\right], \text{ where} \\ \tilde{\nu}_{l,k}^{(s)} &= \breve{\varphi}_{\mathrm{T},k}^{(s-1)} - \frac{\tilde{\kappa}_{\mathrm{T}}^{(s-1)}}{2} + l\tilde{\kappa}_{\mathrm{T}}^{(s)}, \end{aligned} \quad (15)$$

and similarly for $\tilde{\mathbf{U}}_{\mathrm{R},k}^{(s)}$.
3) Construct a new dictionary matrix $\tilde{\boldsymbol{\Omega}}_k^{(s)}[n]$ based on (8) by using $\tilde{\mathbf{U}}_{\mathrm{T},k}^{(s)}$ and $\tilde{\mathbf{U}}_{\mathrm{R},k}^{(s)}$.
4) Based on (9), find a new dictionary index $\tilde{q}_k^{(s)}$ for the corresponding AOD and AOA estimates by using $\tilde{\boldsymbol{\Omega}}_k^{(s)}[n]$ and defining $\mathbf{r}_{s-1}[n] = \mathbf{y}_\varphi[n]$. Now, the new beamspace AOD and AOA estimates can be obtained as

$$\begin{aligned} \breve{\varphi}_{\mathrm{T},k}^{(s)} &= \tilde{\nu}_{\tilde{q}_{\mathrm{T},k}^{(s)}}^{(s)} \text{ and } \breve{\varphi}_{\mathrm{R},k}^{(s)} = \tilde{\nu}_{\tilde{q}_{\mathrm{R},k}^{(s)}}^{(s)}, \text{ where} \\ \tilde{q}_{\mathrm{T},k}^{(s)} &= \left\lceil \frac{\tilde{q}_k^{(s)}}{5} \right\rceil - 1 \text{ and} \\ \tilde{q}_{\mathrm{R},k}^{(s)} &= \mathrm{mod}(\tilde{q}_k^{(s)} - 1, 5). \end{aligned} \quad (16)$$

In addition, for later use in TOA estimation, we denote the $\tilde{q}_k^{(s)\text{th}}$ column vector of $\tilde{\boldsymbol{\Omega}}_k^{(s)}[n]$ as $\tilde{\boldsymbol{\omega}}_k^{(s)}[n]$, which is maximally aligned with the AOD and AOA for the k^{th} path.

5) If the desired beamspace resolution (i.e., $\tilde{\kappa}_{\mathrm{T}}^{(s)}$ and $\tilde{\kappa}_{\mathrm{R}}^{(s)}$) has not yet been reached, repeat from the step 2 by setting $s = s + 1$. Otherwise, obtain the final AOD and AOA estimates for the k^{th} path (in radian) as

$$\begin{aligned} \hat{\varphi}_{\mathrm{T},k} &= \arcsin\left(\frac{\lambda_c}{d_{\text{ant}}}\breve{\varphi}_{\mathrm{T},k}^{(s)}\right) \text{ and} \\ \hat{\varphi}_{\mathrm{R},k} &= \arcsin\left(\frac{\lambda_c}{d_{\text{ant}}}\breve{\varphi}_{\mathrm{R},k}^{(s)}\right). \end{aligned} \quad (17)$$

Remark on complexity: This type of iterative refinement process enables improving the estimation accuracy with a reasonable complexity when compared to using a very large dictionary only once. The fundamental problem of using a large dictionary is that the number of needed dictionary elements grows exponentially as a function of angle resolution. For example, with a single large dictionary, in order to achieve 0.1 degree angle resolution, the required number of dictionary elements for uniformly distributed angles (i.e. the number of columns in $\boldsymbol{\Omega}[n]$) is $(180/0.1)^2 = 3240000$. On the other hand, by assuming $N_{\mathrm{T}} = N_{\mathrm{R}} = 32$ transmit and receive antennas with an orthogonal beamspace, the dictionary size in the DCS-SOMP algorithm is $32^2 = 1024$. After this, by exploiting the above described iterative search process, the 0.1 degree resolution can be achieved with only 6 iterations ($(180/32)/2^6 \approx 0.09$ [deg]), which results in using dictionary matrices with only 25 columns by 6 times per each path during the iterations (e.g., with 3 paths the total number of considered dictionary elements would be $1024 + 3 \times 25 \times 6 = 1474 \ll 3240000$).

C. Estimation of TOA

As shown in [13] and [16], the TOA estimate of each path can be obtained via QR-factorization of the estimated sparse dictionary matrix $\hat{\boldsymbol{\Omega}}[n] = [\hat{\boldsymbol{\omega}}_0^{(s)}[n], ..., \hat{\boldsymbol{\omega}}_{\hat{K}-1}^{(s)}[n]]$, where the columns have been defined at the step 4 in the iterative refinement algorithm. Now, based on the QR-factorization $\hat{\boldsymbol{\Omega}}[n] = \mathbf{Q}[n]\mathbf{R}[n]$, the estimate of the channel vector, incorporating information on each path $k = 0, ..., \hat{K}-1$ at subcarrier n, can be obtained as

$$\begin{aligned} \hat{\mathbf{h}}[n] &= \mathbf{R}^{-1}[n]\tilde{\boldsymbol{\beta}}[n], \text{ with} \\ \tilde{\boldsymbol{\beta}}[n] &= [\tilde{\beta}_0[n], ..., \tilde{\beta}_{\hat{K}-1}[n]], \text{ and} \\ \tilde{\beta}_k[n] &= \frac{\hat{\boldsymbol{\omega}}_k^{(s)H}[n]\mathbf{y}_\varphi[n]}{\|\hat{\boldsymbol{\omega}}_k^{(s)}[n]\|^2}, \end{aligned} \quad (18)$$

where only the first $\hat{K}$ rows of $\mathbf{R}[n]$ (i.e., those with non-zero values) are taken into account. Furthermore, based on the channel model described in (1), the Least Squares (LS) estimate of the TOA for the k^{th} path can be achieved as

$$\begin{aligned} \hat{\tau}_k &= \arg\max_{\tau_k} |\zeta^H(\tau_k)\hat{\tilde{\mathbf{h}}}_k|^2, \text{ where} \\ \zeta^H(\tau_k) &= \left[1, ..., e^{-j2\pi(N-1)\tau_k/(NT_s)}\right]^T \text{ and} \\ \hat{\tilde{\mathbf{h}}}_k &= [\hat{h}_k[0], ..., \hat{h}_k[N-1]]^T, \end{aligned} \quad (19)$$

where $\hat{h}_k[n]$ is the k^{th} element of $\hat{\mathbf{h}}[n]$ given in (18). Now, by using (19), the $\hat{\tau}_k$ can be estimated by trialling different values

of τ_k and choosing the one which maximizes the objective function.

IV. Position and orientation estimation

The statistical descriptions of the unknown parameters (i.e., UE position, scatterer positions and UE orientation) are essential, for example, to approximate the reliability of the obtained parameter estimates, as well as to describe likelihood distributions for Bayesian tracking methods. For this, we perform a sampling procedure based on the estimated AOD, AOA and TOA values obtained in section III. We consider two separate scenarios, where in the first one we assume to have detected the potentially available LOS path, and in the second one we assume that the LOS detection is unavailable with indistinguishable LOS and NLOS paths. Hence, although we do not consider the detection of the LOS path, we provide a novel estimation approach, which can be used for all possible scenarios.

A. Initialization of the positioning process

Since the estimate variances for the AOD, AOA, and TOA are not naturally provided by the DCS-SOMP, we are obligated to determine the estimate uncertainties independently. Due to fairly complicated definitions of estimate variances, we rely on tabulated SNR-dependent variance estimates, obtained from pre-run test simulations over the considered positioning scenario. By using the knowledge of true AOD, AOA and TOA values for each path, the corresponding estimate variances $\sigma^2_{\varphi_{\mathrm{T},k}}$, $\sigma^2_{\varphi_{\mathrm{R},k}}$ and $\sigma^2_{\tau_k}$ are obtained by computing the variances of the resultant error distributions. Since the TOA τ_k is directly proportional to the path distance $d_k = c\tau_k$, the corresponding variance of the path distance estimate $\hat{d}_k$ can be determined as $\sigma^2_{d_k} = \sigma^2_{\tau_k} c^2$.

We assume that the distributions of AOD, AOA and TOA estimates are Gaussian. Due to highly complicated and non-linear dependencies between the estimated UE position $\mathbf{p}_{\mathrm{RX}}$, UE orientation θ, and scatterer positions $\mathbf{p}_{\mathrm{SC},k}$, we exploit the Gibbs sampling method [18] for obtaining the estimates and marginal distributions of the unknown parameters. The fundamental principle of the Gibbs sampler is to sequentially sample each estimated parameter by conditioning it by currently available samples of other parameters. Thus, in order to start the iterative sampling process over $\mathbf{p}_{\mathrm{RX}}$, θ and $\mathbf{p}_{\mathrm{SC},k}$, initialization for at least two parameter samples are required.

If we have successfully detected a LOS path ($k = 0$), it is possible to straightforwardly determine the initial sample for the UE position and orientation based on the estimated AOD, AOA and TOA-based distance $\hat{d}_0 = \hat{\tau}_0 c$ as

$$\begin{aligned} \mathbf{p}^{(0)}_{\mathrm{RX}} &= \begin{bmatrix} \mathbf{p}^{(0)}_{\mathrm{RX,x}} \\ \mathbf{p}^{(0)}_{\mathrm{RX,y}} \end{bmatrix} = \mathbf{p}_{\mathrm{TX}} + \hat{d}_0 \begin{bmatrix} \cos(\hat{\varphi}_{\mathrm{T},0}) \\ \sin(\hat{\varphi}_{\mathrm{T},0}) \end{bmatrix} \\ \theta^{(0)} &= \hat{\varphi}_{\mathrm{T},0} + \hat{\varphi}_{\mathrm{R},0}, \end{aligned} \tag{20}$$

where $\mathbf{p}^{(0)}_{\mathrm{RX,x}}$ and $\mathbf{p}^{(0)}_{\mathrm{RX,y}}$ are the x and y coordinate of the initial UE position sample. Otherwise, without the LOS detection, we sample the initial UE position and orientation by assuming uniformly distributed samples given as

$$\begin{aligned} \mathbf{p}^{(0)}_{\mathrm{RX}} &\sim \begin{bmatrix} \mathcal{U}(x_{\min}, x_{\max}) \\ \mathcal{U}(y_{\min}, y_{\max}) \end{bmatrix} \\ \theta^{(0)} &\sim \mathcal{U}(-\pi/2, \pi/2), \end{aligned} \tag{21}$$

where the limits $x_{\min}$, $x_{\max}$, $y_{\min}$, and $y_{\max}$ restrict the potential area of the UE position (e.g., automatically limited by the path distance based on the TOA estimate).

B. Iterative sampling process for positioning

The iterative sampling process is performed by sequentially sampling each estimated parameter while conditioning it with the currently available samples of other parameters. Hence, until a desired number of samples is obtained, we sample the unknown parameters sequentially in the following order:

1) The scatterer positions $\mathbf{p}_{\mathrm{SC},k}$ for each NLOS path k
2) The UE position $\mathbf{p}_{\mathrm{RX}}$
3) The UE orientation θ

In case that we have observed NLOS paths, or we have a non-detected LOS path which we are forced to consider as a NLOS path, the unknown scatter positions need to be estimated. Thus, we begin the sequential sampling process by taking the i^{th} sample ($i = 1$ for the first iteration) of the scatterer position for each NLOS path. Based on the Gibbs sampling principle, the scatterer position samples are conditioned by the previously sampled UE position $\mathbf{p}^{(i-1)}_{\mathrm{RX}}$ and UE orientation $\theta^{(i-1)}$. First, to facilitate the sampling process, we obtain samples of the AOD, AOA and the path distance from Gaussian distributions given as

$$\begin{aligned} \varphi^{(i)}_{\mathrm{T},k} \sim \mathcal{N}(\hat{\varphi}_{\mathrm{T},k}, \sigma^2_{\varphi_{\mathrm{T},k}}),\ \varphi^{(i)}_{\mathrm{R},k} \sim \mathcal{N}(\hat{\varphi}_{\mathrm{R},k}, \sigma^2_{\varphi_{\mathrm{R},k}}), \\ \text{and } d^{(i)}_k \sim \mathcal{N}(\hat{d}_k, \sigma^2_{d_k}), \end{aligned} \tag{22}$$

respectively. Now, based on the system geometry and the path distance sample $d^{(i)}_k$, the scatterer position can be found somewhere on the ellipse $x^2/a^2 + y^2/b^2 = 1$ with a center point at $(\mathbf{p}_{\mathrm{TX}} + \mathbf{p}^{(i-1)}_{\mathrm{RX}})/2$ and a rotation $\arctan((\mathbf{p}^{(i-1)}_{\mathrm{RX,y}} - \mathbf{p}_{\mathrm{TX,y}})/(\mathbf{p}^{(i-1)}_{\mathrm{RX,x}} - \mathbf{p}_{\mathrm{TX,x}}))$, where

$$\begin{aligned} a &= d^{(i-1)}_k/2, \text{ and} \\ b &= \frac{1}{2}\sqrt{(d^{(i-1)}_k)^2 + \|\mathbf{p}_{\mathrm{TX}} - \mathbf{p}^{(i-1)}_{\mathrm{RX}}\|^2}. \end{aligned} \tag{23}$$

From the ellipse curve, the scatterer position can be determined in two separate ways. For each NLOS path k, based on the the AOD sample and BS position, the first scatterer position candidate $\tilde{\mathbf{p}}^{(i)}_{\mathrm{SCT},k}$, can be found from the intersection of the ellipse and the line going through $\mathbf{p}_{\mathrm{TX}}$ with the slope $\tan(\varphi^{(i)}_{\mathrm{T},k})$. Moreover, based on the samples of AOA, UE position and UE orientation, the second scatterer position candidate $\tilde{\mathbf{p}}^{(i)}_{\mathrm{SCR},k}$ can be found from the intersection of the ellipse and the line going through $\mathbf{p}^{(i-1)}_{\mathrm{RX}}$ with the slope $\tan(\theta^{(i-1)} - \varphi^{(i)}_{\mathrm{R},k})$. If we assume these scatterer position candidates as independent Gaussian variables, the i^{th} scatterer position sample for the k^{th} NLOS path can be obtained as the mean of the joint distribution given as

$$\mathbf{p}^{(i)}_{\mathrm{SC},k} = \frac{\frac{1}{\tilde{\sigma}^2_{\mathrm{SCT},k}}\tilde{\mathbf{p}}^{(i)}_{\mathrm{SCT},k} + \frac{1}{\tilde{\sigma}^2_{\mathrm{SCR},k}}\tilde{\mathbf{p}}^{(i)}_{\mathrm{SCR},k}}{\frac{1}{\tilde{\sigma}^2_{\mathrm{SCT},k}} + \frac{1}{\tilde{\sigma}^2_{\mathrm{SCR},k}}}, \tag{24}$$

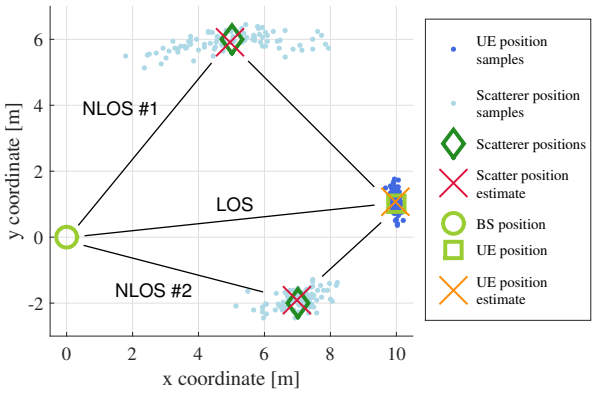

Fig. 2. An example outcome of a sampling process considering the UE position and scatterer position samples with a LOS path and 2 NLOS paths

where $\tilde{\sigma}^2_{\text{SC,T}} = \sigma^2_{d_k} + \sigma^2_{\varphi_{\text{T},k}}$ and $\tilde{\sigma}^2_{\text{SC,R}} = \sigma^2_{d_k} + \sigma^2_{\varphi_{\text{R},k}}$ are approximated variances for the candidate scatterer positions. The approximated variances are based on the sum of variances of the corresponding path distance and angle estimates used to determine the candidate scatterer positions.

Next, we proceed to obtain the i^{th} sample of the UE position, which is now conditioned by the current scatterer position samples $\mathbf{p}^{(i)}_{\text{SC},k}$ of all NLOS paths and the previous UE orientation sample $\theta^{(i-1)}$. Again, for each path k, in order to facilitate the sampling process, we take new samples of AOD, AOA, and the path distance as described in (22), denoted as $\tilde{\varphi}^{(i)}_{\text{T},k}$, $\tilde{\varphi}^{(i)}_{\text{R},k}$ and $\tilde{d}^{(i)}_k$, respectively.

In case of a detected LOS path, a UE position sample candidate $\tilde{\mathbf{p}}^{(i)}_{\text{RX},0}$ can be obtained similarly as done in (20), but replacing the estimated parameter values $\hat{d}_0$ and $\hat{\varphi}_{\text{T},0}$ with the corresponding sample values $\tilde{\varphi}^{(i)}_{\text{T},0}$ and $\tilde{d}^{(i)}_0$. Furthermore, for each NLOS path, we are able to achieve a UE position sample candidate as

$$\tilde{\mathbf{p}}^{(i)}_{\text{RX,k}} = \mathbf{p}^{(i)}_{\text{SC,k}} + \tilde{d}^{(i)}_{2,k} \begin{bmatrix} \cos(\theta^{(i-1)} - \tilde{\varphi}^{(i)}_{\text{R},k}) \\ \sin(\theta^{(i-1)} - \tilde{\varphi}^{(i)}_{\text{R},k}) \end{bmatrix} \text{ with } \tilde{d}^{(i)}_{2,k} = \tilde{d}^{(i)}_k - \tilde{d}^{(i)}_{1,k}, \tag{25}$$

where $\tilde{d}^{(i)}_{1,k} = \|\mathbf{p}_{\text{TX}} - \mathbf{p}^{(i)}_{\text{SC,k}}\|$ and $\tilde{d}^{(i)}_{2,k}$ are the samples of partial path distances (i.e., the distances from BS to scatterer and from scatterer to UE). Now, similar to (24), the i^{th} UE position sample is approximated by using a weighted mean as

$$\mathbf{p}^{(i)}_{\text{RX}} = \left(\sum_{\tilde{k}=0}^{\hat{K}-1} \frac{1}{\tilde{\sigma}^2_{\text{RX},\tilde{k}}} \right)^{-1} \sum_{k=0}^{\hat{K}-1} \frac{1}{\tilde{\sigma}^2_{\text{RX},k}} \tilde{\mathbf{p}}^{(i)}_{\text{RX},k} \tag{26}$$

where we approximate $\tilde{\sigma}^2_{\text{RX},k} = \sigma^2_{d_k} + \sigma^2_{\varphi_{\text{R},k}}$, except for the possible LOS path $\tilde{\sigma}^2_{\text{RX},0} = \sigma^2_{d_0} + \sigma^2_{\varphi_{\text{T},0}}$.

The last unknown to be sampled at the i^{th} iteration is the UE orientation, which is now conditioned by the current scatterer position samples $\mathbf{p}^{(i)}_{\text{SC},k}$ (only for the NLOS paths) and UE position sample $\mathbf{p}^{(i)}_{\text{RX}}$. Again, based on (22), we begin by obtaining samples of the AOD and AOA as $\check{\varphi}^{(i)}_{\text{T},k}$, $\check{\varphi}^{(i)}_{\text{R},k}$. Now, for a detected LOS path ($k = 0$), the UE orientation sample candidate can be obtained as $\tilde{\theta}^{(i)}_k = \check{\varphi}^{(i)}_{\text{T},0} + \check{\varphi}^{(i)}_{\text{R},0}$. Then, for any NLOS path k the UE orientation sample candidate can be given as

$$\tilde{\theta}^{(i)}_k = \arctan\left(\frac{\mathbf{p}^{(i)}_{\text{RX,y}} - \mathbf{p}^{(i)}_{(\text{SC},k),\text{y}}}{\mathbf{p}^{(i)}_{\text{RX,x}} - \mathbf{p}^{(i)}_{(\text{SC},k),\text{x}}} \right) + \check{\varphi}^{(i)}_{\text{R},k} \tag{27}$$

where $\mathbf{p}^{(i)}_{(\text{SC},k),\text{y}}$ and $\mathbf{p}^{(i)}_{(\text{SC},k),\text{y}}$ are the x and y coordinate of the $\mathbf{p}^{(i)}_{\text{SC},k}$. Analogously with the scatterer position and UE position sampling, the UE orientation samples are approximated as a weighted mean of the sample candidates as

$$\theta^{(i)} = \left(\sum_{\tilde{k}=0}^{\hat{K}-1} \frac{1}{\tilde{\sigma}^2_{\theta,\tilde{k}}} \right)^{-1} \sum_{k=0}^{\hat{K}-1} \frac{1}{\tilde{\sigma}^2_{\theta,k}} \tilde{\theta}^{(i)}_k \tag{28}$$

where the approximated sample candidate variances are defined as $\tilde{\sigma}^2_{\theta,0} = \sigma^2_{\varphi_{\text{T},0}} + \sigma^2_{\varphi_{\text{R},0}}$ for a LOS path and $\tilde{\sigma}^2_{\theta,k} = \sigma^2_{\varphi_{\text{R},k}}$ for a NLOS path.

After acquiring the i^{th} UE orientation sample, we are able to proceed to the next sampling iteration ($i = i + 1$) to obtain new samples for the scatterer positions by conditioning with the updated UE position and UE orientation samples from the previous iteration round. The process continues until a desired number of samples has been obtained. After this, the parameter estimates can be obtained by simply computing the mean of the corresponding sample distributions. In Fig. 2 we illustrate the sampled UE and scatterer positions of one arbitrary outcome of the sampling process with SNR$= -8$ dB. In this scenario we consider a LOS path and two NLOS paths with scatterer positions at $\mathbf{p}_{\text{RX}} = [5, 6]^T$ and $\mathbf{p}_{\text{RX}} = [7, -2]^T$. Furthermore, the BS is located at the origin and the UE is found at $\mathbf{p}_{\text{RX}} = [10, 1]^T$ (m) with the orientation of 25 degrees.

V. Positioning and Channel Parameter Estimation Performance

For the simulations we consider two separate path propagation scenarios based on the channel geometry depicted in Fig. 2. In the first scenario (denoted as "LOS only"), only the LOS path is considered available, and in the second scenario (denoted as "LOS+2×NLOS"), the LOS path and both of the 2 NLOS paths are available. For the transmission we use a carrier frequency of $f_c = 60$ GHz with a bandwidth of $B = 200$ MHz, where $N = 20$ active sub-carriers uniformly distributed to the band are used for the positioning purposes. The number of transmit and receive antennas is given as $N_{\text{T}} = N_{\text{R}} = 32$ with the UE antenna orientation of $\theta = 25$ deg. The transmitted signal includes $M = 32$ OFDM symbols with Quadrature Phase Shift Keying (QPSK) modulated subcarriers, and the beamforming matrix $F[m, n]$ is defined so that during the $M = 32$ OFDM symbols, the beam directions are uniformly distributed from $-\pi/2$ to $\pi/2$. We do not consider any UE mobility or UE tracking, and hence, the channel geometry and path availability are fixed throughout the simulations. Furthermore, we determine the path loss coefficient based on the free-space path loss model, and introduce an additional reflection loss of 6 dB for the NLOS paths.

For the AOD and AOA estimation, we employ uniformly sampled angles in the DCS-SOMP algorithm. After this, for the

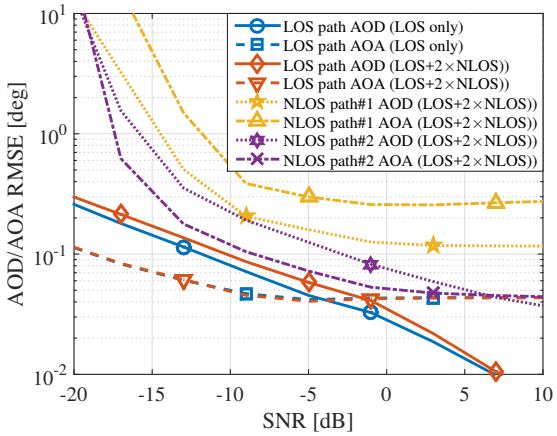

Fig. 3. Estimation RMSE for the AOD and AOA of each path by considering the LOS only and LOS+2×NLOS scenarios

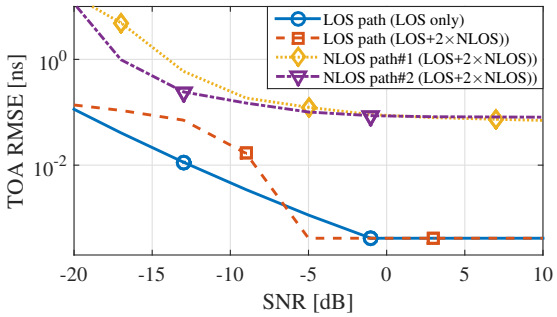

Fig. 4. Estimation RMSE for the TOA of each path by considering the LOS only and LOS+2×NLOS scenarios

$\hat{K}$ found paths, we use 3 iterative refinement steps to improve the angle estimation accuracy. Moreover, the resolution of the search grid used in the TOA estimation is 1/6 ns. In the UE position and orientation estimation, we utilize 10000 samples with the Gibbs sampler, from where we discard the first 100 samples to avoid dependency on the initialization effects, and use only every 20^{th} sample in order to minimize the correlation between adjacent samples. Finally, all the presented results are averaged over 1000 Monte Carlo realizations.

In Fig. 3, we show and compare the AOD and AOA estimation Root Mean Square Error (RMSE) as a function of SNR for each path in the considered LOS and LOS+2×NLOS scenarios. Here, as well as with the following results, the SNR is defined as the ratio between the total power of the received signal (just before the noise addition) and the total power of the noise. As excepted, the LOS paths provide the best estimation accuracy, since due to the reflection losses and the shortest path lengths, they have significantly higher received power compared to NLOS paths. Moreover, the differences in estimation accuracy between the AOD and AOA of the same path are explained by the system geometry and the considered UE orientation. The corresponding TOA estimation RMSE is shown in Fig. 4. It can be seen that an error floor, originating from the used grid-based search method, is reached with high SNR values. However, from the positioning point of view, the error floor does not have a large impact on the positioning

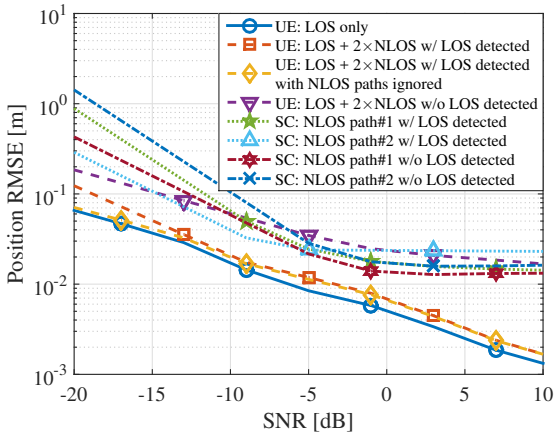

Fig. 5. Estimation RMSE for the UE and scatterer (SC) position by considering the LOS only and LOS+2×NLOS scenarios including distinct LOS detection information and handling of NLOS paths.

accuracy, until the accuracy of the AOD and AOA estimates is sufficiently high.

The UE position estimation RMSE for the LOS and LOS+2×NLOS scenarios are shown in Fig. 5. In addition, for the latter scenario also the scatterer position estimate RMSE is provided for both paths. Excluding the LOS only scenario, we have considered 3 separate approaches for the positioning. In the first approach we assume a perfect LOS detection and use both the LOS and NLOS paths in the estimation process. In the second case, we also assume the LOS detection, but we completely ignore the NLOS paths in the estimation process. Finally, in the last approach, we assume that the LOS detection is unavailable, and therefore we consider each path as a NLOS path. In the latter case the position of the non-existent scatterer of the LOS path is likely to be found somewhere on the line between the BS and UE. From the system geometry point of view, this is not optimal for the position estimation, as the covariance of the scatterer position estimate is very large in direction of the line between the BS and UE. It can be seen that without the LOS detection, the scatterer position estimates are within the same level of accuracy with the UE position estimate. Nonetheless, based on the considered system configuration, including NLOS paths in the estimation process seems not to offer any gain to the estimation accuracy. Similar observations can be achieved by considering the corresponding results for the UE orientation estimation RMSE, shown in Fig. 6. It is worth noticing that when using NLOS paths in the estimation, additional unknown parameters (i.e. scatterer positions) are introduced, which results in more challenging estimation task. However, the achievable positioning accuracy is very high, independently of the considered LOS and NLOS aspects.

VI. Conclusion

In this paper, we presented methods for estimating the position and orientation of UE in a single BS scenario. Based on the sparsity of the considered mm-wave channel, we used compressive sensing approach to obtain coarse AOD, AOA, and TOA estimates for each observed propagation path without assuming the knowledge of the number of propagation paths.

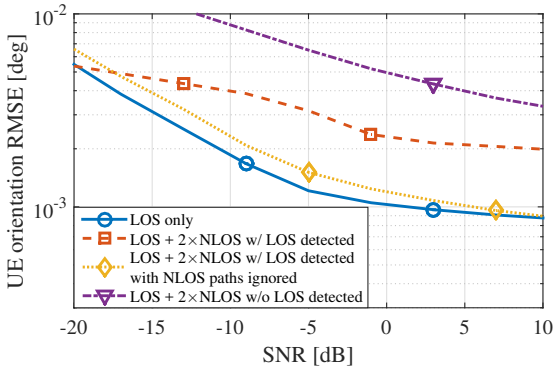

Fig. 6. Estimation RMSE for the UE orientation by considering the LOS only and LOS+2×NLOS scenarios including distinct LOS detection information and handling of NLOS paths.

After this, we employed an iterative refinement method, in which the resolution of the sparse dictionary was increased in order to improve the accuracy of the coarse estimates. Based on the obtained channel parameters, we derived an iterative Gibbs sampler, where we sequentially sampled the unknown system parameters, including the positions of the UE and the scatterers, as well as the UE orientation. Moreover, after drawing a sufficient number of samples, statistical descriptions and the corresponding estimates of the unknown parameters were obtained.

The presented results showed that the proposed approach can facilitate a centimeter-level estimation accuracy for the UE and scatterer positioning regardless of the available LOS path or LOS path detection. In addition, the achieved estimation accuracy of less than 1 degree for the UE orientation was comparable with the accuracy of the AOD and AOA estimates. Furthermore, it was observed that using the detected NLOS paths was not able to improve the positioning performance when compared to using only the LOS path.

Besides UE positioning, the knowledge of scatterer positions and their statistical descriptions, can prove to be a valuable asset in 5G communications when considering mobility and the resulted time-dependent channel conditions. For example, when the LOS path availability, or the consistency of the LOS path detection, is compromised, NLOS paths offer diversity for the communications and positioning. Moreover, by continuously tracking the scatterer positions, it is possible to quickly react to changes in LOS availability and LOS detection, and additionally, to facilitate radio resource management functionalities, such as location and channel aware beamforming.

ACKNOWLEDGMENT

This work is financially supported by the Finnish Funding Agency for Innovation (Tekes), under the project "Wireless for Verticals" (WIVE), and by the Horizon2020 projects 5GCAR and HIGHTS MG-3.5a-2014-636537, the VINNOVA COPPLAR project, funded under Strategic Vehicle Research and Innovation Grant No. 2015-04849.

REFERENCES

[1] M. Agiwal, A. Roy, and N. Saxena, "Next generation 5g wireless networks: A comprehensive survey," *IEEE Communications Surveys Tutorials*, vol. 18, no. 3, pp. 1617–1655, thirdquarter 2016.

[2] T. S. Rappaport, S. Sun, R. Mayzus, H. Zhao, Y. Azar, K. Wang, G. N. Wong, J. K. Schulz, M. Samimi, and F. Gutierrez, "Millimeter wave mobile communications for 5g cellular: It will work!," *IEEE Access*, vol. 1, pp. 335–349, 2013.

[3] Z. Marzi, D. Ramasamy, and U. Madhow, "Compressive channel estimation and tracking for large arrays in mm-wave picocells," *IEEE Journal of Selected Topics in Signal Processing*, vol. 10, no. 3, pp. 514–527, April 2016.

[4] N. Garcia, H. Wymeersch, E. G. Strm, and D. Slock, "Location-aided mm-wave channel estimation for vehicular communication," in *2016 IEEE 17th International Workshop on Signal Processing Advances in Wireless Communications (SPAWC)*, July 2016, pp. 1–5.

[5] G. Destino, M. Juntti, and S. Nagaraj, "Leveraging sparsity into massive mimo channel estimation with the adaptive-lasso," in *2015 IEEE Global Conference on Signal and Information Processing (GlobalSIP)*, Dec 2015, pp. 166–170.

[6] Z. Guo, X. Wang, and W. Heng, "Millimeter-wave channel estimation based on two-dimensional beamspace music method," *IEEE Transactions on Wireless Communications*, vol. PP, no. 99, pp. 1–1, 2017.

[7] Hua Deng and A. Sayeed, "Mm-wave mimo channel modeling and user localization using sparse beamspace signatures," in *2014 IEEE 15th International Workshop on Signal Processing Advances in Wireless Communications (SPAWC)*, June 2014, pp. 130–134.

[8] S. Park and R. W. Heath, "Frequency selective hybrid precoding in millimeter wave ofdma systems," in *2015 IEEE Global Communications Conference (GLOBECOM)*, Dec 2015, pp. 1–6.

[9] J. Choi, "On coding and beamforming for large antenna arrays in mm-wave systems," *IEEE Wireless Communications Letters*, vol. 3, no. 2, pp. 193–196, April 2014.

[10] S. Hur, T. Kim, D. J. Love, J. V. Krogmeier, T. A. Thomas, and A. Ghosh, "Millimeter wave beamforming for wireless backhaul and access in small cell networks," *IEEE Transactions on Communications*, vol. 61, no. 10, pp. 4391–4403, October 2013.

[11] K. Witrisal, P. Meissner, E. Leitinger, Y. Shen, C. Gustafson, F. Tufvesson, K. Haneda, D. Dardari, A. F. Molisch, A. Conti, and M. Z. Win, "High-accuracy localization for assisted living: 5g systems will turn multipath channels from foe to friend," *IEEE Signal Processing Magazine*, vol. 33, no. 2, pp. 59–70, March 2016.

[12] J. Saloranta and G. Destino, "On the utilization of mimo-ofdm channel sparsity for accurate positioning," in *2016 24th European Signal Processing Conference (EUSIPCO)*, Aug 2016, pp. 748–752.

[13] A. Shahmansoori, G. E. Garcia, G. Destino, G. Seco-Granados, and H. Wymeersch, "5g position and orientation estimation through millimeter wave mimo," in *2015 IEEE Globecom Workshops (GC Wkshps)*, Dec 2015, pp. 1–6.

[14] A. Guerra, F. Guidi, and D. Dardari, "Position and orientation error bound for wideband massive antenna arrays," in *2015 IEEE International Conference on Communication Workshop (ICCW)*, June 2015, pp. 853–858.

[15] J. H. Brady and A. M. Sayeed, "Wideband communication with high-dimensional arrays: New results and transceiver architectures," in *2015 IEEE International Conference on Communication Workshop (ICCW)*, June 2015, pp. 1042–1047.

[16] M. F. Duarte, S. Sarvotham, D. Baron, M. B. Wakin, and R. G. Baraniuk, "Distributed compressed sensing of jointly sparse signals," in *Conference Record of the Thirty-Ninth Asilomar Conference onSignals, Systems and Computers, 2005.*, October 2005, pp. 1537–1541.

[17] J. Brady, N. Behdad, and A. M. Sayeed, "Beamspace mimo for millimeter-wave communications: System architecture, modeling, analysis, and measurements," *IEEE Transactions on Antennas and Propagation*, vol. 61, no. 7, pp. 3814–3827, July 2013.

[18] C. Riggelsen, *Approximation Methods for Efficient Learning of Bayesian Networks*, Dissertations in artificial intelligence. IOS Press, 2006.